

Cation-Mediated Acid-Base Pairs for Mild Oxidative Cleavage of Lignocellulosic β -1,4-Glycosidic Bonds

Hongguang Zhang,^a Aiguo Wang,^a Ruixuan Zhao,^b and Jinguang Hu^{a,*}

Solar-driven lignocellulosic biomass photoreforming holds significant promise for the production of value-added chemicals and fuels. The cleavage of the β -1,4-glycosidic bond is crucial for the effective conversion of lignocellulosic biomass. Polymeric carbon nitride (PCN) with acid-base pairs (M-C sites) is developed through heteroatomic carbon incorporation and cation insertion. It can be used for the gentle oxidation of cellobiose to monosaccharides, bypassing the formation of organic acids such as gluconic acid and glucaric acid. A series of different alkaline/alkaline-earth cation for regulation of acid-base pairs exhibited a negative correlation between β -1,4-glycosidic bond cleavage and cation radii. In particular, the introduction of short-radius cations (such as Li) into PCN enabled the formation of acid-base (M-C) pairs characterized by strong acidity. It also enhanced electron delocalization around M-C sites, potentially promoting the generation of reactive radicals in the reaction. Electron paramagnetic resonance analysis confirmed the presence of \bullet OH radicals. The mild oxidative species, are the primary reactive radicals responsible for β -1,4-glycosidic bond cleavage in cellobiose. This study provides insightful evidence for the rational regulation of acid-base sites in facilitating β -1,4-glycosidic bond cleavage. It sheds light on the oxidative cleavage mechanisms integral to lignocellulosic biomass photoreforming, offering insights for advancing sustainable biomass conversion technologies.

DOI: 10.15376/biores.19.2.2736-2748

Keywords: Alkaline/alkaline-earth cation regulation; Acid-base pairs; β -1,4-Glycosidic bond; Gentle-oxidative cleavage; Cellobiose photoreforming

Contact information: a: Department of Chemical and Petroleum Engineering, University of Calgary, 2500 University Drive, NW, Calgary, Alberta T2N1N4, Canada; b: Institute of Food Science and Technology, Chinese Academy of Agricultural Sciences, Comprehensive Key Laboratory of Agro-products Processing, Ministry of Agriculture and Rural Affairs, Beijing 100193, PR China;

* Corresponding author: jinguang.hu@ucalgary.ca

INTRODUCTION

Lignocellulosic biomass valorization into value-added chemicals and fuels offers a promising alternative to renewable energy source production. Currently, biomass industrial treatment primarily relies on traditional chemical engineering technologies, such as thermochemical and biological processes. These approaches generally require extra additives and energy input, posing challenges to economic sustainability (Wang *et al.* 2021; Zhao *et al.* 2022). In contrast, solar-driven biomass valorization into valuable chemicals and fuels has attracted great attention due to the beauty of solely using clean solar irradiation as the energy source (Zhang *et al.* 2022). Over the past years, successful demonstrations illustrated the feasibility of solar-driven conversion of biomass building block (such as glucose) into gluconic acid (Wang *et al.* 2023), lactic acid (Ma *et al.* 2021), and others. However, these studies mainly focused on the basic organic feedstocks derived

from biomass. A clear mechanistic investigation into the key β -1,4-glycosidic bond in the cellulose chain is missing, which hinders the future application of lignocellulosic biomass valorization *via* photocatalysis. Addressing this knowledge gap is crucial for enhancing the efficiency and applicability of solar-driven biomass conversion techniques and unlocking the full potential of solar-driven biomass valorization, thereby contributing to sustainable and economically viable alternatives to traditional energy sources.

Cellulose, a polymer of glucose units linked by β -1,4-glycosidic bonds, is the most abundant biomass feedstock in nature, accounting for approximately 40 to 45% of raw materials (Zhu *et al.* 2023; Covinich and Area 2024). Cellobiose, the structural building block of cellulose, is a glucose dimer linked by β -1,4-glycosidic bonds and represents the predominant repetitive unit of cellulose (Sarip *et al.* 2016). Therefore, gaining insightful understanding into the mechanism of photocatalytic cellobiose conversion would provide significant foresight for cellulose photoreforming. Recent investigations on the direct photoconversion of cellobiose into glucaric acid (Zhao *et al.* 2022) or gluconic acid (Wang *et al.* 2024) revealed that the reaction pathway involves the formation of strong oxidation radicals (such as $\bullet\text{O}_2^-$) for the oxidative cleavage of the β -1,4-glycosidic bond. Through uncovering alternative pathways that do not rely on these strong oxidative processes, exploring the gentle-oxidative pathway for β -1,4-glycosidic bond cleavage in cellobiose is essential for expanding the universal application of lignocellulosic biomass valorization.

As illustrated in Fig. 1a, during the biocatalytic conversion of polysaccharides, chemically modified enzymes, such as lytic polysaccharide monooxygenases (Munzone *et al.* 2024), are observed to form acid-base pairs (copper-oxyl ($\text{Cu(II)}-\text{O}\bullet$) reactive species) through cationization conjugation for the cleavage of cellobiose glycosidic bonds. Inspired by the cationization conjugation mechanism, a similar strategy was employed to incorporate potassium ions (K^+) into the framework of C-doped graphitic carbon nitride (g- C_3N_4) for the formation of K-C pairs. The resulting K-C pairs demonstrated excellent Lewis acid-base properties (Zhang *et al.* 2022). Therefore, it is hypothesized that rational cation incorporation combined with heteroatomic doping into the g- C_3N_4 framework could regulate the chemical activity of acid-base sites, achieving the cellobiose photoreforming *via* mild oxidative cleavage of the β -1,4-glycosidic bond. Additionally, the resulting catalysts are solid powders, making them easy to separate from the reaction media. By simplifying the separation process through methods such as filtration or centrifugation, catalyst recovery significantly reduces costs and time associated with complex separation techniques, enhancing cost-effectiveness and time-efficiency in large-scale applications. Moreover, catalyst recovery promotes resource conservation and sustainability by enabling catalyst reuse, thereby reducing waste generation and environmental impact.

In this work, a g- C_3N_4 photocatalyst with acid-base pairs (derived from M-C pairs) was prepared by chemically heteroatomic C doping and metal cation (M) insertion into the g- C_3N_4 framework for mild oxidative photoconversion of cellobiose into monosaccharides. Various alkaline metal or alkaline-earth metal cations, known for their strong electron attraction ability, were utilized to synthesize g- C_3N_4 photocatalysts with different M-C pairs. Cellobiose was converted into glucose and fructose monomer under the facilitation of a modified g- C_3N_4 photocatalyst. The effect of acid-base pairs (derived from M-C pairs) on the β -1,4-glycosidic bond cleavage in cellobiose was investigated. The results indicated that cations with shorter ionic radius exhibited stronger electron delocalization from adjacent C atoms, resulting in enhanced acidity of acid-base (M-C) sites. An electron paramagnetic resonance (ESR) analysis revealed that $\bullet\text{OH}$ radicals played a primary role in the gentle-oxidative cleavage of β -1,4-glycosidic bonds *via* photocatalysis. This work

provides insightful evidence of rational regulation of acid-base pair sites for gentle-oxidative cleavage of β -1,4-glycosidic bonds, offering promising prospects for the development of efficient and sustainable biomass valorization processes.

EXPERIMENTAL

Materials

All of the chemicals were used without further purification. Melamine ($C_3H_6N_6$, 99%, Sigma), 2,4,6-triamine-pyrimidine ($C_4H_7N_5$, TAP, 97%, Sigma), lithium chloride ($LiCl$, $\geq 99\%$, Sigma), sodium chloride ($NaCl$, $\geq 99\%$, Sigma), potassium chloride (KCl , $\geq 99\%$, Sigma), rubidium chloride ($RbCl$, $\geq 99\%$, Sigma), magnesium chloride ($MgCl_2$, anhydrous, $\geq 98\%$, Sigma), calcium chloride ($CaCl_2$, anhydrous, $\geq 97\%$, Sigma), strontium chloride hexahydrate ($SrCl_2$, 99%, Sigma), barium chloride ($BaCl_2$, 99.9%, Sigma), and ethanol (C_2H_5OH , AR, Sigma) were used.

Methods

Modified polymeric carbon nitride (PCN) was prepared by the procedures described in the authors' previously published work (Zhang *et al.* 2022). Typically, a mixture of 2.0 g melamine, 4.0 g $LiCl$, and 2.0 g TAP was finely ground, with the addition of 2 mL ethanol, for 10 min. Then, ethanol was evaporated at 80 °C to obtain the well-mixed powder. The precursor mixture was then transferred into a crucible with cover and annealed at 600 °C for 3 h with a ramp rate of 3 °C/min in the furnace under air atmosphere. After cooling down, the crude sample powder was fully immersed into boiling water to remove residual $LiCl$. Finally, the product was collected and vacuum-dried at 60 °C overnight.

Different cation incorporated PCN was prepared following above procedure, except for $LiCl$ replacement.

Pristine g- C_3N_4 was prepared at the same condition as PCN by only using melamine as a precursor.

Characterizations

Power X-ray diffraction (XRD)

The crystal phase was measured by a power X-ray diffractometer (XRD, D8 ADVANCE) equipped with a Cu anode X-ray tube (Cu $K\alpha$ X-rays, $\lambda = 1.54056 \text{ \AA}$).

Field-emission scanning electron microscopy (SEM)

The morphology was measured by a SEM (Hitachi S-4800), and the surface topography of was observed by an accelerating voltage of 3 kV.

Transmission electron microscopy (TEM)

The morphology and lattice space were determined by a TEM (JEOL JEM 2100 F) with an accelerating voltage of 200 kV, equipped with a field emission analytical electron microscope.

X-ray photoelectron spectra (XPS)

The chemical elements components and state were performed with an X-ray photoelectron spectrometer (Thermo Fisher, Alpha equipped with a monochromatic Al K α source) and all the raw data were calibrated by C (1 s) at 284.8 eV.

Fourier-transform infrared spectra (FTIR)

The specific chemical groups of prepared samples were measured by FTIR with a PerkinElmer Frontier instrument in the range of 4000 to approximately 500 cm⁻¹.

Ultraviolet-visible (UV-vis) diffuse reflectance spectra (UV-vis DRs)

The UV-vis DRs were recorded by a SHIMADZU UV-vis spectrophotometer in the range of 200 to approximately 900 nm.

NH₃ temperature-programmed desorption (NH₃-TPD)

The NH₃ temperature-programmed desorption (NH₃-TPD) measurements were carried out on AutoChem II 2920 Version (USA). Prior to performing the experiment, the catalyst sample was pretreated by He gas to remove impurity absorbed on the surface. After that, a gas mixture (10% NH₃/ He with a flow rate of 30 to 50 mL/min) was purged into the system for 1 h to be saturated state. Finally, high-purity He was changed and heated up to 500 °C with a ramp of 10 °C/min. The desorbed gas was measured by TCD of GC.

Electron paramagnetic resonance (ESR) spectra

The active groups were measured by an ESR spectroscope, and the active groups of prepared samples were investigated by DMPO for •O₂⁻ and •OH detection under dark and illumination, respectively.

Photocurrent Measurement

Photocurrent density of prepared samples was recorded by an electrochemical workstation (CHI 660E) with a standard three-electrode system. The as-prepared FTO glass loading photocatalyst was used as the working electrodes, a Pt slice electrode as the counter electrode, and an Ag/AgCl as the reference electrode, respectively. The 0.5 M Na₂SO₄ solution was used as electrolyte. A 300 W Xenon lamp (PLS-SXE300D, Beijing Perfectlight) was used as the light source. For the FTO electrode preparation, 15 mg prepared samples were dispersed into 0.5 mL Nafion/ethanol solution ($V_{\text{nafion}}:V_{\text{ethanol}} = 25:475$) and then made in an ultrasonic treatment for 20 min. Subsequently, 20 μ L of prepared solution was dropped onto the surface of FTO glass (the working surface area was 1.0×1.0 cm²). Then, the electrode was dried at room temperature to volatilize the solution naturally.

Photocatalytic Performance Measurement and Product Qualification

For cellobiose photoreforming, photocatalytic tests were conducted using a 20-mL glass vial. A volume of 10 mL cellobiose solution of 1.0 g/L was mixed evenly with 15 mg of catalyst. Prior to running the photocatalytic reaction, the glass vial containing cellobiose solution and catalyst was placed in darkness and stirred for 0.5 h, after that, the reactions were initiated by a 300 W Xenon lamp for 1h with light intensity of 1 W/cm². The reaction temperature was approximately 60 °C. After reaction, the photocatalyst powder was removed from the liquid products solution by centrifugation. The dark trial over PCN(Li) and the experiment without a photocatalyst were conducted under the same conditions.

The yield of products was calculated using Eq. 2 (Wang *et al.* 2024):

$$Yield_{\text{Glucose/Fructose}} = \frac{\text{Concentration of Glucose or Fructose}}{\text{Initial concentration of cellobiose}} \times \frac{1}{2} \times 100\% \quad (2)$$

The possible products were analyzed *via* a refractive index detector (RID) along with a high-performance liquid chromatography (HPLC, 1200 Agilent) column and an Aminex HPX-87 H column (300 × 7.8 mm, Bio-Rad). The mobile phase was sulfuric acid (H₂SO₄) at 0.6 mL/min flow rate with a concentration of 5 mM.

RESULTS AND DISCUSSION

Catalyst Characterizations

The PCN was prepared through a salt-template-inducing method, where exogenous carbon was incorporated into the heptazine framework of g-C₃N₄. Because of its superior electron-donating properties compared to nitrogen, exogenous carbon was introduced into g-C₃N₄ framework as a replacement for intrinsic nitrogen to construct effective acid-base sites through electron delocalization. As illustrated in Fig. 1b (inset), the similar unit structure of melamine and TAP facilitates the incorporation of carbon into the basic framework of g-C₃N₄ during the copolymerization process.

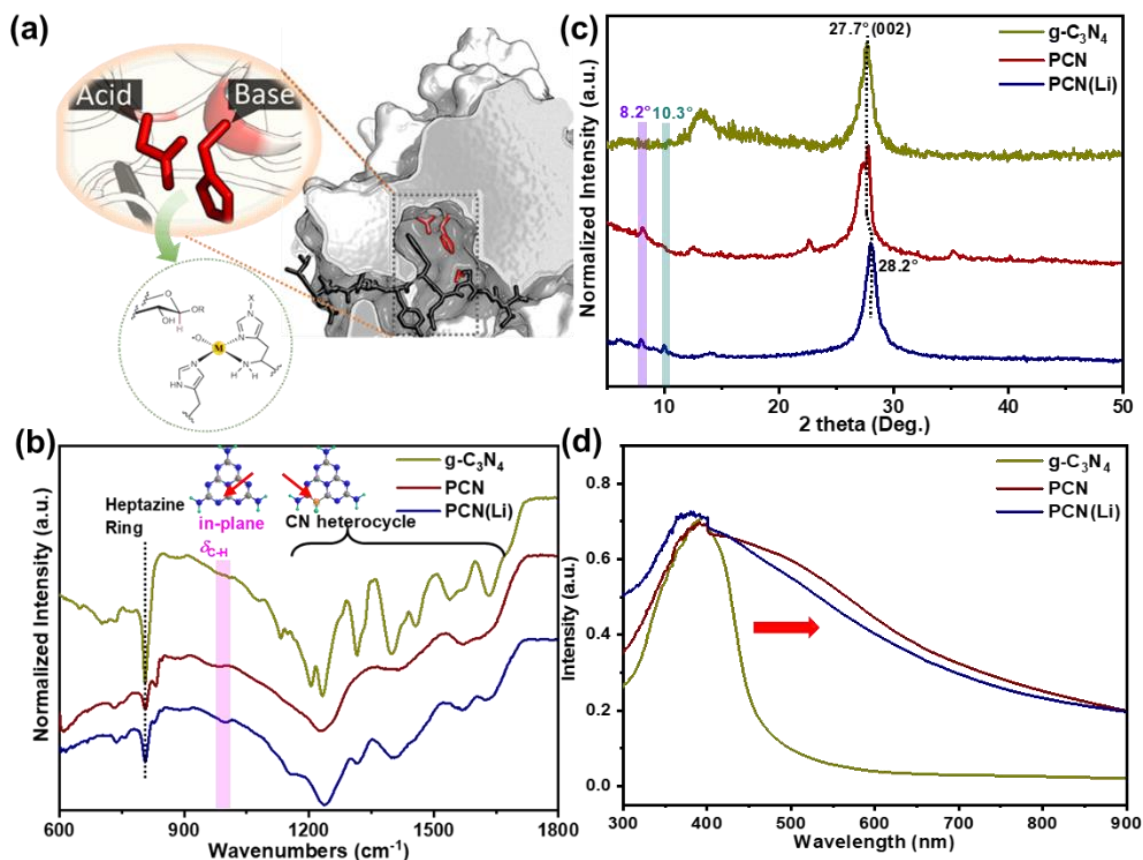


Fig. 1. Structural illustration of acid-base site derived from cationization conjugation in enzyme (a); FTIR spectra (b, inset: chemical structure of melamine (left) and TAP (right); gray: C; blue: N; cyan: H; orange: highlight C in TAP), XRD patterns (c), and UV-vis DRs spectra (d) of prepared pristine g-C₃N₄, PCN, and PCN(Li)

Compared to $g\text{-C}_3\text{N}_4$, the new peak at around 992 cm^{-1} in the FTIR spectra of PCN and PCN(Li) (Fig. 1b) is ascribed to in-plane C-H bending mode ($\delta_{\text{C-H}}$), implying the successful incorporation of carbon into the TAP polymer (Xu *et al.* 2021; Zhang *et al.* 2022). The similar fingerprint peaks at 805 cm^{-1} and in the range from 1150 to 1700 cm^{-1} correspond to the vibration mode of the heptazine ring and stretching and bending modes of the conjugated CN heterocycles, respectively (Zhang *et al.* 2018). These peaks are observed in all catalysts, suggesting that the salt-template approach has little influence on the basic framework of $g\text{-C}_3\text{N}_4$.

As shown in Fig. 1c, two new peaks are evident at 8.2° and 10.3° in the XRD pattern of PCN(Li), which are assigned to the configuration of crystal facets deriving from heteroatomic C and Li (Zhang *et al.* 2022). The lattice spacing of the (002) facet in PCN(Li) was observed to shift slightly from 27.7° to 28.2° compared to $g\text{-C}_3\text{N}_4$ and PCN. These observations confirm that the isolation effect of LiCl crystal size and Li insertion into the PCN framework. Interestingly, in comparison to $g\text{-C}_3\text{N}_4$ (Fig. 1d), C incorporation and Li insertion contribute to the defective level in PCN, resulting in the red shift of light absorbance edge (Xu *et al.* 2021; Zhang *et al.* 2022).

The inserted metal ions (*e.g.*, Li) combine with heteroatomic C to construct a metal-nonmetal (Li-C) acid-base pairs, similar to acid-base pairs (copper-oxyl: $\text{Cu(II)-O}\bullet$) in Fig. 1a. The formed acid-base could act as chemically favorable sites for the cleavage of β -1,4-glycosidic bonds.

The $g\text{-C}_3\text{N}_4$ and PCN display the bulk, nonporous crystal structures shown in Figs. 2a and 2b. However, the morphology of PCN(Li) showed a porous structure, which probably can be attributed to the isolation effect of LiCl salt template (Fig. 2c inset) during the copolymerization process. The porous structure of PCN(Li) could potentially offer more active acid-base sites available for the adsorption of cellobiose. The HRTEM images in Fig. 2d further confirm the specific crystal structure in PCN(Li), where the lattice space of 0.325 nm belongs to the (002) facet of carbon nitride (Ma *et al.* 2022).

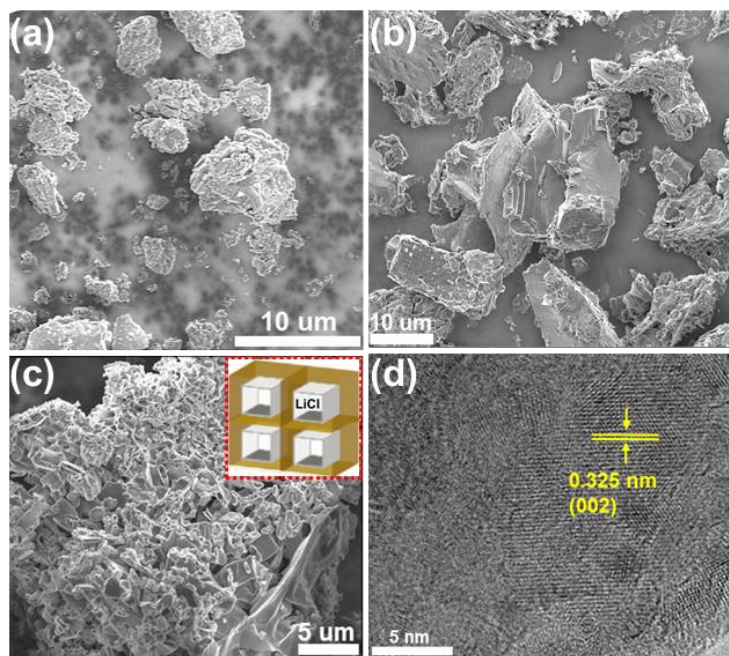


Fig. 2. SEM images of $g\text{-C}_3\text{N}_4$ (a), PCN (b), and PCN(Li) (c), and HRTEM image of PCN(Li) (d)

The chemical state and structure of the as-prepared photocatalysts were further examined with XPS techniques. The survey spectra (Fig. 3a) illustrated the presence of both N and C in all catalysts. Compared to g-C₃N₄ and PCN, the Li signal was exclusively observed in PCN(Li) due to Li incorporation into PCN framework. Three peaks at the 284.6, 285.9, and 288.4 eV in the C 1s spectra (Fig. 3b) correspond to C=C/C-C, C≡N/C-O, and N-C=N groups in the structure of g-C₃N₄, respectively (Wang *et al.* 2019; Zhang *et al.* 2022). Interestingly, compared to g-C₃N₄, the peak area of C=C/C-C and C≡N/C-O in both PCN and PCN(Li) was larger, which is indicative of higher C doping in PCN and PCN(Li) (Xu *et al.* 2021). In addition, the peak position for both PCN (at 288.2 eV) and PCN (Li) (at 287.8 eV) shifts towards lower binding energy compared to g-C₃N₄ (288.4 eV). The observed shift in PCN (0.2 eV) is attributed to the replacement of nitrogen (N) with carbon (C) that possesses a higher electron delocalization ability. The more noticeable shift in PCN (Li) (0.8 eV) is ascribed to Li⁺ insertion, as Li⁺ has a stronger electron attraction, leading to the electron cloud of C (gray in Fig. 3b) and N (blue in Fig. 3b) deviating toward nearby C (green in Fig. 3b) in the TAP unit. Three peaks appearing at 398.9, 400.3, and 404.7 eV in the N 1s XPS spectra (Fig. 3c) originate from the heptazine unit (C-N=C), tertiary nitrogen (N-C₃), and terminal amino (C-NH_x), respectively (Wang *et al.* 2019; Ma *et al.* 2022). Conversely, C doping and Li insertion leads to a high-energy peak shift in both PCN and PCN(Li). The Li 1s spectra of PCN(Li) (Fig. 3d) strongly supports Li incorporation into PCN. The XPS analysis is consistent with the observations from FTIR and XRD. In summary, heteroatomic C incorporation and Li attraction render the photocatalyst with more active M-C (Li-C) acid-base sites, facilitating the gentle oxidative conversion of cellobiose.

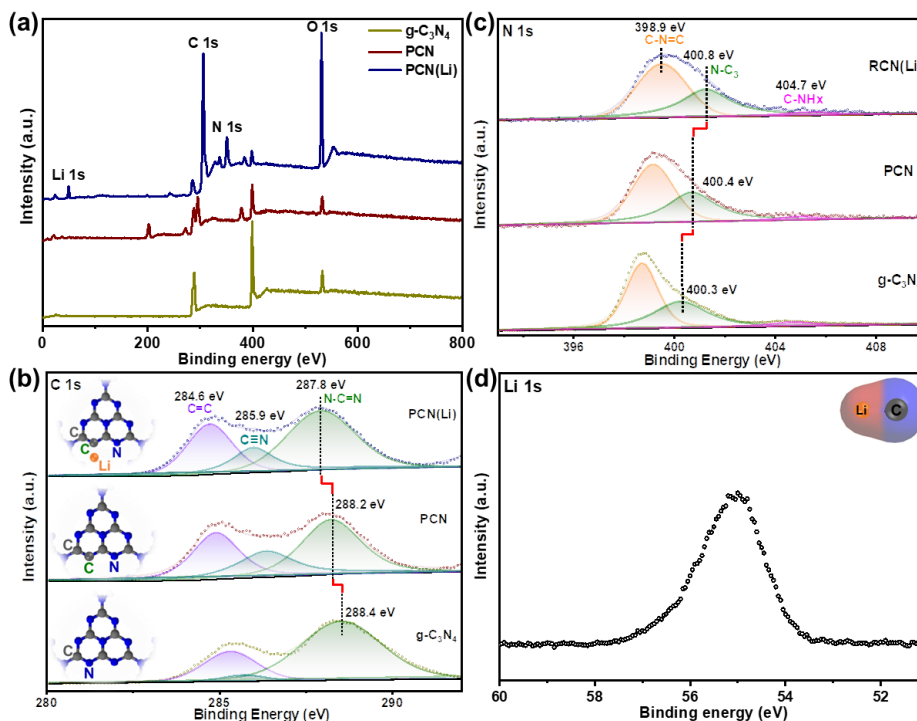


Fig. 3. XPS survey spectra (a), high-resolution N 1s spectra (b), high-resolution C 1s spectra of g-C₃N₄, PCN, and PCN(Li) (c inset: Top-Li insertion with TAP unit in PCN(Li), middle-TAP unit in PCN; bottom-heptazine unit in g-C₃N₄); and high-resolution Li 1s spectra of PCN (Li) (d) (inset: schematic illustration of Li-C (M-C) acid-base site)

Photocatalytic Performance

Various PCN(M) photocatalysts with acid-base (M-C) pair were prepared using alkaline metal or alkaline-earth metal salt as precursors for the cleavage of β -1,4-glycosidic bond in cellobiose. The photocatalytic performance of as-synthesized catalysts on cellobiose conversion was evaluated under full-spectrum illumination. As shown in Fig. 4a and 4b, glucose and fructose were identified as the major products from cellobiose photoconversion. Glucose and fructose are probably produced by the mild oxidative cleavage of an intermediate derived from cellobiose on acid-based pairs. There was a trace amount of glucose and fructose produced from cellobiose photoconversion over PCN or g-C₃N₄, while the incorporation of metal species in PCN enhanced cellobiose photoconversion, leading to the formation of more monosaccharide products. Compared to PCN (M=Rb, Ca, Sr, Ba), a higher yield of glucose and fructose was obtained over PCN (M=Li, Na, K, Mg). The correlation between the product yield and metal species is presented in Fig. 4c.

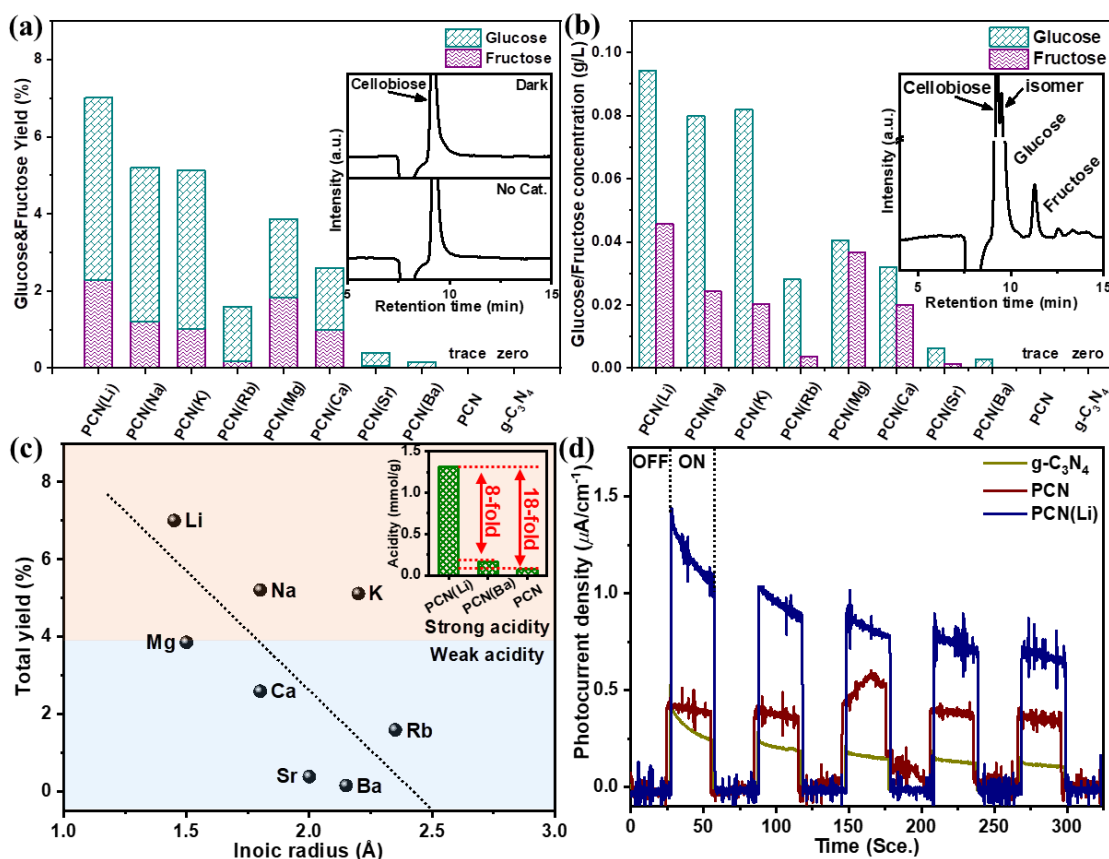


Fig. 4. Glucose and Fructose yield (a, inset: no photocatalyst (bottom) and dark (top) control experiment conducted over PCN(Li)), and corresponding glucose and fructose concentration from photocatalytic cellobiose conversion over different catalysts (b); correlation diagram between total yield of glucose and fructose and ionic radius (c inset: acidity measurement of PCN(Li), PCN(Ba) and PCN based on the NH₃ adsorption) (Strong/weak acidity represents acidity of formed acid-base pairs (M-C)); transient photocurrent of g-C₃N₄, PCN, and PCN(Li) (d)

It appears that the incorporation of a cation with a short radius (such as Li, Na, K, or Mg) into PCN gave a higher yield compared to metal species (such as Rb, Ca, Sr, or Ba) with long radius. PCN(Li) showed the best performance on cellobiose photoconversion to

glucose and fructose due to its shortest radius. The incorporation of short-radius cations into PCN enables the formation of acid-base (M-C) pairs with strong acidity. Metal species with a short radius typically demonstrate strong electron attraction, resulting in enhanced electron delocalization around M-C sites. In addition, NH₃-TPD measurements were conducted over PCN(Li), PCN(Ba), and PCN. As shown in Fig.4c inset, the present findings indicated that metal insertion increased surface acidity, with distinct effects observed for different metal species. Specifically, Li insertion exhibited a remarkable amount of NH₃ adsorption compared to Ba insertion and PCN without metal ion insertion. These results are consistent with the observation in Fig. 4c that the incorporation of short-radius cations (such as Li) into PCN enables the formation of acid-base (M-C) pairs with strong acidity.

When exposed to light, the delocalized electrons around M-C (*e.g.*, Li-C) sites potentially promote the formation of reactive radicals responsible for β -1,4-glycosidic bond cleavage, as evidenced by higher photocurrent density over PCN (Li) in Fig. 4d. The dark trail, experiments without photocatalyst, and the reaction with g-C₃N₄ or PCN were conducted under the same conditions. HPLC analysis (Fig. 4a) showed that there were no detectable products from cellobiose conversion without illumination or a photocatalyst, whether using g-C₃N₄ or PCN as the photocatalyst. These results indicate that the acid-base pair derived from the synergy of cations and adjacent carbon played a crucial role in the gentle oxidative cleavage of β -1,4-glycosidic bonds.

Mechanism Analysis

The photogenerated reactive radicals play a significant role in biomass photoconversion, such as superoxide radical ($\bullet\text{O}_2^-$) or hydroxyl radical ($\bullet\text{OH}$) (Zhao *et al.* 2022; Wang *et al.* 2023). An ESR analysis was conducted to identify and characterize the free radicals involved in the β -1,4-glycosidic bond cleavage in cellobiose over PCN(Li). As shown in Fig. 5a and 5b, there was no signal indicating the generation of reactive radicals in the absence of light irradiation. Upon light illumination, the signals due to $\bullet\text{O}_2^-$ and $\bullet\text{OH}$ radicals were clearly detected. Moreover, the intensity of $\bullet\text{O}_2^-$ radicals signal was much weaker than that of $\bullet\text{OH}$ radicals signal, implying that $\bullet\text{OH}$ radicals are the primary reactive radicals responsible for the β -1,4-glycosidic bond cleavage. Previous work reported the photogenerated $\bullet\text{O}_2^-$ radicals for the oxidative cleavage of β -1,4-glycosidic bond to produce organic acids such as gluconic acid and glucaric acid (Zhao *et al.* 2022; Wang *et al.* 2024). Compared to $\bullet\text{O}_2^-$ radicals, $\bullet\text{OH}$ radicals showed weaker oxidation ability, therefore, resulting in the formation of glucose and fructose as the main products from the cleavage of the β -1,4-glycosidic bond in cellobiose (Fig. 4a and 4b).

Both IPA and 1,4-benzoquinone (BQ) serve as scavengers for $\bullet\text{OH}$ and $\bullet\text{O}_2^-$ radicals, respectively. As shown in Fig. 5c, the product yield decreases with the addition of scavengers in the reaction. However, there was a notable difference in the product yield between the cases of adding IPA and BQ. Specifically, the product yield was higher when using BQ compared to the product yield when IPA was added. This comparison repeatedly confirmed that the photogenerated $\bullet\text{OH}$ radicals were the main reactive radicals for β -1,4-glycosidic bond cleavage in cellobiose.

Based on these observations, a possible pathway for the cleavage of β -1,4-glycosidic bond in cellobiose over PCN(Li) is proposed in Fig. 5d. Initially, the formation of acid-base pairs (M-C) in PCN provides favorable adsorption and isomerization sites for saccharides (Zhang *et al.* 2022). Thus, cellobiose is transformed into its isomer (glucose-fructose) on acid-base sites (confirmed by HPLC analysis in Fig. 4b inset). Subsequently,

the oxygen atom of the β -1,4-glycosidic bond in the isomer combines with an acidic proton to form the corresponding conjugated acid (intermediate II), weakening the β -1,4-glycosidic bond. The photogenerated $\cdot\text{OH}$ radicals then cleave the weakened β -1,4-glycosidic bond to produce glucose and fructose as the final products (Yu *et al.* 2013; Wang *et al.* 2024).

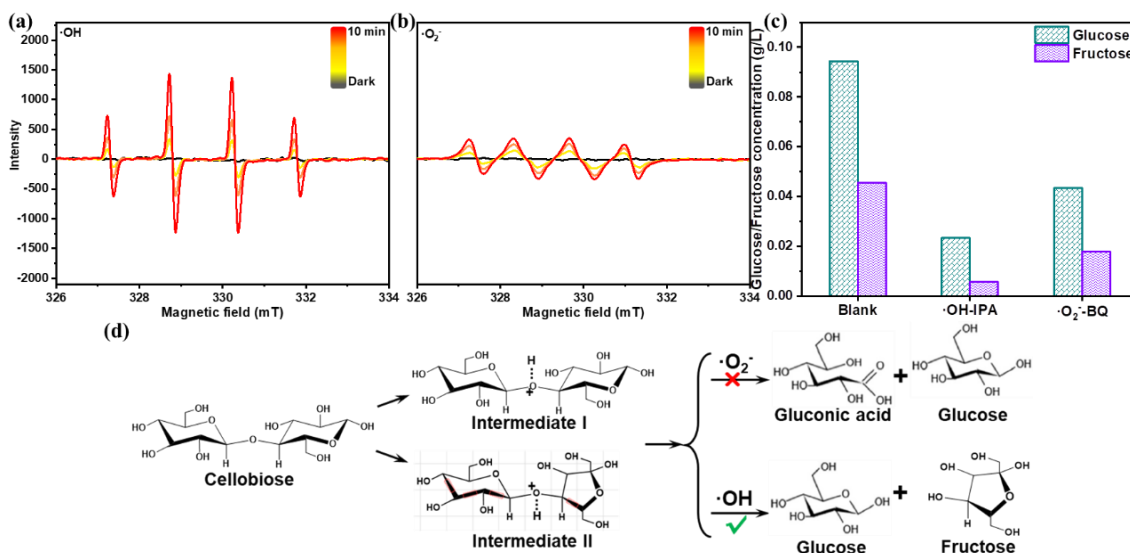


Fig. 5. Time-resolved ESR spectra of DMPO- $\cdot\text{O}_2^-$ (a) and DMPO- $\cdot\text{OH}$ (b) for PCN(Li) photocatalyst, and the effect of different scavengers for photocatalytic cellobiose conversion (c), schematic pathway illustration of in β -1,4-glycosidic bond cleavage in cellobiose by photocatalysis (d)

Building upon the insights from photocatalysis, the potential of combining photo and bio refining techniques is explored, as illustrated in Fig. 6. This concept is rooted in the production of photoinduced electrons and oxidative radicals observed during the photocatalysis mechanism. Such a system holds promise for various biorefining applications. Specifically, co-factor (NADH/NAD⁺)-dependent biosystems could harness photoinduced electrons for processes like the shuttle process (I), exemplified by formate dehydrogenase. Additionally, oxidoreductases could directly utilize radicals to facilitate biorefining processes (II), demonstrated by lytic polysaccharide monooxygenases, among others. These processes underscore the promising synergy between photocatalysis and biorefining, paving the way for innovative and sustainable solutions.

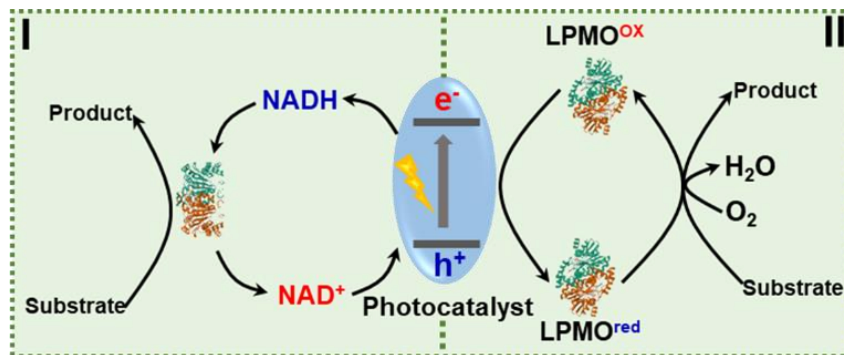


Fig. 6. Schematic illustration of potential photo-bio hybrid system

CONCLUSIONS

Various metal-associated polymeric carbon nitride photocatalysts (PCN(M)) featuring acid-base (M-C) pairs were prepared for usage in the gentle cleavage of the β -1,4-glycosidic bond in cellobiose. The effect of cation insertion on the activity of acid-base (M-C) sites was investigated by assessing the photocatalytic performance on cellobiose conversion.

1. The incorporation of heteroatomic C into PCN enhanced the local electron-donating ability, while metal cation insertion improved the electron delocalization of C-C-N bonds. This synergistic effect of metal cations and heteroatomic C contributed to the formation of acid-base (M-C) sites conducive to β -1,4-glycosidic bond cleavage.
2. A negative correlation was established between the efficiency of photocatalytic β -1,4-glycosidic bond cleavage and ionic radius, indicating that stronger acidity of acid-base sites (M-C) is associated with smaller ionic radii.
3. \bullet OH radicals were identified as the primary participants in the photocatalytic cleavage of the β -1,4-glycosidic bond in a mild oxidative way.
4. The reaction pathway of cellobiose photoconversion likely involves cellobiose isomerization and the formation of a conjugated acid intermediate, followed by the cleavage of the weakened β -1,4-glycosidic bond by the photogenerated \bullet OH radicals to produce glucose and fructose.

These findings provide valuable insights into the mechanisms underlying the photocatalytic cleavage of the β -1,4-glycosidic bond in cellobiose, offering potential avenues for the development of efficient and sustainable biomass conversion technologies.

ACKNOWLEDGEMENTS

The authors are grateful for financial support of Canada First Research Excellent Funds (J.H.), and China Scholarship Council scholarship (H. Z.).

REFERENCE CITED

- Covinich, L. G., and Area, M. C. (2024). "Trends and limitations of lignin as a starting material," *BioResources* 19(1), 6-9. DOI: 10.15376/biores.19.1.6-9
- Crystal Maker (2024). "Elements, Atomic Radii and the Periodic Table," Crystal Maker Software, (www.crystallmaker.com/support/tutorials/atomic-radii/index.html), Accessed 01 December 2023.
- Ma, J. L., Jin, D. N., Li, Y. C., Xiao, D. Q., Jiao, G. J., Liu, Q., Guo, Y. Z., Xiao, L. P., Chen, X. H., Li, X. Z., *et al.* (2021). "Photocatalytic conversion of biomass-based monosaccharides to lactic acid by ultrathin porous oxygen doped carbon nitride," *Applied Catalysis B: Environmental* 283, article ID 119520. DOI: 10.1016/j.apcatb.2020.119520
- Ma, X. M., Ma, Z., Zhang, H. G., Lu, D. Z., Duan, J. Z., and Hou, B. R. (2022). "Interfacial Schottky junction of Ti₃C₂T_x MXene/g-C₃N₄ for promoting spatial charge

- separation in photoelectrochemical cathodic protection of steel,” *Journal of Photochemistry and Photobiology A: Chemistry* 426, article ID 113772. DOI: 10.1016/j.jphotochem.2022.113772
- Munzone, A., Eijssink, V. G. H., Berrin, J. G., and Bissaro, B. (2024). “Expanding the catalytic landscape of metalloenzymes with lytic polysaccharide monoxygenases,” *Nature Reviews Chemistry* 8, 106-119. DOI: 10.1038/s41570-023-00565-z
- Sarip, H., Sohrab Hossain, M., Azemi M. N. M., and Allaf, K. (2016). “A review of the thermal pretreatment of lignocellulosic biomass towards glucose production: Autohydrolysis with DIC technology,” *BioResources* 11(4) 10625-10653. DOI: 10.15376/biores.11.4.Sarip
- Wang, J., Chen, L., Zhao, H., Kumar, P., Larter, S. R., Kibria, Md. G., and Hu, J. G. (2023). “*In Situ* photo-Fenton-like tandem reaction for selective gluconic acid production from glucose photo-oxidation,” *ACS Catalysis* 13(4) 2637-2646. DOI: 10.1021/acscatal.2c05931
- Wang, J., Zhao, H., Chen, L., Björk, J., Rosen, J., Kumar, P., Jing, L. Q., Chen, J., Kibria, Md. G., and Hu, J. G. (2024). “Selective cellobiose photoreforming for simultaneous gluconic acid and syngas production in acidic conditions,” *Applied Catalysis B: Environmental* 344, article ID 123665. DOI: 10.1016/j.apcatb.2023.123665
- Wang, J., Zhao, H., Zhu, B. C., Larter, S., Cao, S. W., Yu, J. G., Kibria, Md. G., and Hu, J. G. (2021). “Solar-driven glucose isomerization into fructose *via* transient Lewis acid-base active sites,” *ACS Catalysis* 11(19) 12170-12178. DOI: 10.1021/acscatal.1c03252
- Wang, L., Zhang, H. G., Guo, C. Y., Feng, L. J., Li, C. H., and Wang, W. T. (2019). “Facile constructing plasmonic Z-scheme Au NPs/g-C₃N₄/BiOBr for enhanced visible light photocatalytic activity,” *Journal of Fuel Chemistry and Technology* 47(7), 834-842. DOI: 10.1016/S1872-5813(19)30036-2
- Xu, Y. S., Fan, M. J., Yang, W. J., Xiao, Y. H., Zeng, L. T., Wu, X., Xu, Q. H., Su, C. L., and He, Q. J. (2021). “Homogeneous carbon/potassium-incorporation strategy for synthesizing red polymeric carbon nitride capable of near-infrared photocatalytic H₂ production,” *Advanced Materials* 33(39), article ID 2101455. DOI: 10.1002/adma.202101455
- Yu, Y., Shafie, Z. M., and Wu, H. W. (2013). “Cellobiose decomposition in hot-compressed water: Importance of isomerization reactions” *Industrial & Engineering Chemistry Research* 52(47), 17006-17014. DOI: 10.1021/ie403140q
- Zhang, H. G., Feng, L. J., Li, C. H., and Wang, L. (2018). “Preparation of graphitic carbon nitride with nitrogen-defects and its photocatalytic performance in the degradation of organic pollutants under visible light,” *Journal of Fuel Chemistry and Technology* 46(7) 871-878. DOI: 10.1016/S1872-5813(18)30036-7
- Zhang, H. G., Zhao, H., Zhai, S. X., Zhao, R. X., Wang, J., Cheng, X., Shiran, H. S., Larter, S., Kibria, Md. G., and Hu, J. G. (2022). “Electron-enriched Lewis acid-base sites on red carbon nitride for simultaneous hydrogen production and glucose isomerization,” *Applied Catalysis B: Environmental* 316, article ID 121647. DOI: 10.1016/j.apcatb.2022.121647
- Zhao, H., Li, C. F., Yu, X. T., Zhong, N., Hu, Z. Y., Li, Y., Larter, S., Kibria, Md. G., and Hu, J. G. (2022). “Mechanistic understanding of cellulose β -1,4-glycosidic cleavage via photocatalysis,” *Applied Catalysis B: Environmental* 302, article ID 120872. DOI: 10.1016/j.apcatb.2021.120872

Zhu, L. X., Liang, K. Z., Wang, M., Xing, T., Chen, C. X., and Wang, Q. L. (2023).
“Microwave-assisted formic acid/cold caustic extraction for separation of cellulose
and hemicellulose from biomass,” *BioResources* 18(4), 6896-6912. DOI:
10.15376/biores.18.4.6896-6912

Article submitted: February 8, 2024; Peer review completed: February 24, 2024; Revised
version received: February 29, 2024; Accepted: March 2, 2024; Published: March 14,
2024.

DOI: 10.15376/biores.19.2.2736-2748